

# An Innovative Experiment to Test a Paradigm-Shifting Theory in Physics through Alteration of Light Speed in Electromagnetic Interactions

Wim Vegt

Department of Physics

Eindhoven University of Technology

The Netherlands

[wimvegt@quantumlight.science](mailto:wimvegt@quantumlight.science)



## Abstract

The foundation of Einstein's General Relativity lies in the curvature of spacetime due to gravitational fields, emphasizing a constant speed of light in vacuum. In contrast, a novel perspective rooted in "Equilibrium" for the five fundamental force densities in light posits varying light speeds when coherent laser beams intersect, challenging General Relativity's constant light speed assumption. This research delves into the interaction between gravity and light at astronomical and sub-atomic levels, branching into Gravitational Redshift, Black Holes, and Dark Matter, alongside microscopic phenomena of light absorption and emission.

Unlike General Relativity, this new viewpoint unites gravity and light through a synthesis of the Stress-Energy Tensor and the Gravitational Tensor. It elucidates Gravitational-Electromagnetic Interaction, unveiling a tensor representation for Black Holes (Gravitational Electromagnetic Confinements) through the interplay of electromagnetic energy gradients and Lorentz transformations. By incorporating the "CURL" effect within gravitational fields near Black Holes, this theory surpasses the explanatory power of General Relativity, particularly in Gravitational Lensing scenarios.

Einstein's groundwork, featuring the Einstein Gravitational Constant within the Energy-Stress Tensor, contrasts with this reinterpretation presenting the combined Electromagnetic Tensor and Gravitational Tensor. Theoretical advancements in Black Hole solutions echo John Archibald Wheeler's pioneering work in 1955, offering fundamental solutions for the relativistic quantum mechanical Dirac equation in tensor formalism. Experimental validation of this paradigm shift, conducted with Galileo Satellites and ground-based measurements of MASER frequency, underscores the discrepancies between General Relativity and the New Theory in predicting

Gravitational Redshift, pushing the boundaries of gravitational observations beyond modern accuracies.

The convergence of Quantum Physics and General Relativity theories, exemplified by approaches like String Theory, predicts variable natural constants. This interdisciplinary endeavor stands to redefine perspectives on the gravitational constant "G," illustrating its constancy over time when bridging the realms of General Relativity and Quantum Physics.

This abstract encapsulates the essence of groundbreaking research into the interplay of light, gravity, and theoretical frameworks, promising potential breakthroughs at the forefront of optical and gravitational sciences..

**Keywords**

Quantum Physics, General Relativity, Gravitational RedShift, Black Holes, Dark Matter

## 1. An alternative approach in Gravity

Einstein approached the interaction between gravity and light by the introduction of the “Einstein Gravitational Constant” in the 4-dimensional Energy-Stress Tensor.

$$\mathbf{G}_{\mu\nu} + \Lambda \mathbf{g}_{\mu\nu} = \kappa \mathbf{T}_{\mu\nu} \quad (1)$$

In which  $\mathbf{G}_{\mu\nu}$  equals the Einstein Tensor,  $\mathbf{g}_{\mu\nu}$  equals the Metric Tensor,  $\mathbf{T}_{\mu\nu}$  equals the Stress-Energy tensor,  $\Lambda$  equals the cosmological constant and  $\kappa$  equals the Einstein gravitational constant.

An alternative approach to Einstein’s expression with the tensor  $\kappa \mathbf{T}_{\mu\nu}$ , describing the curvature of the Space-Time continuum, is the sum of the Electromagnetic Tensor  $\mathbf{T}_{\mu\nu}$  and the Gravitational Tensor  $\mathbf{J}_{\mu\nu}$ .

$$\kappa \mathbf{T}_{\mu\nu} \Leftrightarrow \mathbf{T}_{\mu\nu} + \mathbf{J}_{\mu\nu} \quad (2)$$

The 4-dimensional divergence of the sum of the Electromagnetic Stress-Energy tensor and the Gravitational Tensor expresses the 4-dimensional Force-Density vector (expressed in  $[\text{N/m}^3]$  in the 3 spatial coordinates) as the result of Electro-Magnetic-Gravitational interaction.

$$f^\mu = \partial_\nu \left( \mathbf{T}^{\mu\nu} + \mathbf{J}^{\mu\nu} \right) \quad (3)$$

In vector notation the 4-dimensional Force-Density vector can be written as:

$$\vec{f}^4 = \begin{pmatrix} f_4 \\ f_3 \\ f_2 \\ f_1 \end{pmatrix} = \square \cdot \left( \vec{\vec{T}} + \vec{\vec{J}} \right) \quad (4)$$

The fundamental boundary condition for this alternative approach to gravity is the requirement that the Force 4 vector equals zero in the 4 dimensions, expressing a universal 4-dimensional equilibrium:

$$\vec{f}^4 = \begin{pmatrix} f_4 \\ f_3 \\ f_2 \\ f_1 \end{pmatrix} = \square \cdot (\vec{T} + \vec{J}) = \vec{0}^4 \quad (5)$$

The 3 spatial components of the Force-Density vector, as a result of Electro-Magnetic-Gravitational interaction can be written as:

$$\begin{aligned} \vec{f} = & -\frac{1}{c^2} \frac{\partial (\vec{E} \times \vec{H})}{\partial t} + \epsilon_0 \vec{E} (\nabla \cdot \vec{E}) - \epsilon_0 \vec{E} \times (\nabla \times \vec{E}) + \\ & + \mu_0 \vec{H} (\nabla \cdot \vec{H}) - \mu_0 \vec{H} \times (\nabla \times \vec{H}) + \gamma_0 \vec{g} (\nabla \cdot \vec{g}) - \gamma_0 \vec{g} \times (\nabla \times \vec{g}) = \vec{0} \quad [\text{N/m}^3] \end{aligned} \quad (6)$$

in which:  $\mu_0 (\nabla \cdot \vec{H}) = \rho_M$  Magnetic Flux Density [Vs/ m<sup>3</sup>] or [Wb/ m<sup>3</sup>]

$\gamma_0 (\nabla \cdot \vec{g}) = \rho_M$  Mass Density (Electromagnetic) [kg/ m<sup>3</sup>]

Electric Energy Density:  $w_E = \frac{1}{2} \epsilon_0 E^2$

Magnetic Energy Density:  $w_M = \frac{1}{2} \mu_0 H^2$

Gravitational Energy Density:  $w_G = \frac{1}{2} \gamma_0 g^2$

In which E represents the electric field intensity expressed in [V/m], H represents the magnetic field intensity expressed in [A/m] and g represents the gravitational acceleration expressed in [m/s<sup>2</sup>]. The permittivity indicated as  $\epsilon_0$ , the permeability indicated as  $\mu_0$  and the gravitational permeability of vacuum as  $\gamma_0$ .

For curl-free gravitational fields equation (6) can be written as:

$$\begin{aligned} \vec{f} = & -\frac{1}{c^2} \frac{\partial (\vec{E} \times \vec{H})}{\partial t} + \epsilon_0 \vec{E} (\nabla \cdot \vec{E}) - \epsilon_0 \vec{E} \times (\nabla \times \vec{E}) + \\ & + \mu_0 \vec{H} (\nabla \cdot \vec{H}) - \mu_0 \vec{H} \times (\nabla \times \vec{H}) + \vec{g} \rho_M = \vec{0} \quad [\text{N/m}^3] \end{aligned} \quad (7)$$

Substituting Einstein's  $W = m c^2$  in (7) results in “Electro-Magnetic-Gravitational Equilibrium Field Equation” (8):

$$\begin{aligned} \bar{f} = & -\frac{1}{c^2} \frac{\partial (\bar{\mathbf{E}} \times \bar{\mathbf{H}})}{\partial t} + \varepsilon_0 \bar{\mathbf{E}} (\nabla \cdot \bar{\mathbf{E}}) - \varepsilon_0 \bar{\mathbf{E}} \times (\nabla \times \bar{\mathbf{E}}) + \\ & + \mu_0 \bar{\mathbf{H}} (\nabla \cdot \bar{\mathbf{H}}) - \mu_0 \bar{\mathbf{H}} \times (\nabla \times \bar{\mathbf{H}}) + \frac{1}{2c^2} \bar{g} (\varepsilon E^2 + \mu H^2) = \bar{0} \quad [\text{N/m}^3] \end{aligned} \quad (8)$$

The theory describes “Electromagnetic-Gravitational Interaction”, “Magnetic-Gravitational Interaction” and “Electric-Gravitational Interaction”. In this new theory particles do not interact with fields. The interaction between an electric charged particle and an electric field is not the interaction between a particle and a field but it is the interaction between the electric field of the particle interacting with the other electric field. Every interaction is an interaction between fields. Electric Fields interact with Electric Fields, Magnetic Fields interact with Magnetic Fields and Gravitational Fields interact with Gravitational Fields.

## 2 “Gravitational RedShift/ BlueShift in “Light (EMR)” due to “Electromagnetic Gravitational Interaction”

To test the New Theory, the Gravitational-Redshift experiment: “Test of the Gravitational Redshift with Galileo Satellites in an Eccentric Orbit” by S. Hermann et al, has been chosen [2]. In this experiment a stable “MASER” frequency from a ground station has been emitted to 2 Galileo Satellites, measuring the frequency difference between the Ground Station and the Satellites. The frequency shift has been caused by the gravitational field of the Earth and 2 satellites has been chosen to compensate for the eccentricity of the Galileo Orbit.

Assuming a gravitational field  $g[z]$  depending on the radial direction in cartesian coordinates between the ground station and the satellites:

$$\overline{g[z]} = \left\{ 0, 0, \frac{G M_{Earth}}{4 \pi z^2} \right\} \quad (9)$$

In which  $G$  ( $G = 6.67428 \cdot 10^{-11} \text{ Nm}^2 / \text{kg}^2$ ) equals the Gravitational constant,  $M_{Earth}$  the mass of the earth and  $r$  the radial distance from the centre of the earth. The mathematical solution [5] of equation (8) for plane electromagnetic waves (expressed in cartesian  $\{x, y, z\}$  coordinates) related to the Electric Field Intensity equals:

$$\vec{E} = \begin{pmatrix} E_x \\ E_y \\ E_z \end{pmatrix} = \begin{pmatrix} e^{-\frac{G M_{Earth} \epsilon_0 \mu_0}{8 \pi z}} h \left[ \omega_0 e^{-\frac{G M_{Earth} \epsilon_0 \mu_0}{4 \pi z}} (t - \sqrt{\epsilon \mu} z) \right] \\ 0 \\ 0 \end{pmatrix} \quad (10)$$

And the mathematical solution of (8) for the Magnetic Field Intensity equals:

$$\vec{H} = \begin{pmatrix} H_x \\ H_y \\ H_z \end{pmatrix} = \begin{pmatrix} 0 \\ \frac{1}{\sqrt{\epsilon_0 \mu_0}} e^{-\frac{G M_{Earth} \epsilon_0 \mu_0}{8 \pi z}} h \left[ \omega_0 e^{-\frac{G M_{Earth} \epsilon_0 \mu_0}{4 \pi z}} (t - \sqrt{\epsilon \mu} z) \right] \\ 0 \end{pmatrix} \quad (11)$$

In which  $\omega_0$  equals the original frequency of the MASER radiation propagating in the direction of the gravitational field  $g[z]$  of the Earth in the  $z$ -direction. The exponential term demonstrates the Gravitational Redshift when the MASER radiation propagates in the direction of the Gravitational Field of the earth. The propagation speed of the Electromagnetic Radiation remains constant (the speed of light). But the amplitude of the field intensity and the frequency of the field intensity diminishes exponentially.

Calculations in Mathematica [5] demonstrate a difference between the calculation with General Relativity and the calculation with the New Theory. Choosing for the ground station a distance to the centre of the earth  $z_1 = 6,378,000$  [m] (Radius of the Earth) and for the average distance of the ESA satellites in a Galileo orbit  $z_2 = 23,222,000$  [m] (distance from the ESA satellite to the centre of the Earth), calculated with Mathematica, the Gravitational RedShift according General Relativity equals:

$$\Delta \omega_{GR} = 0.00000000004011815497097883 \text{ [s}^{-1}\text{]} \quad (12)$$

Calculated with Mathematica, the Gravitational RedShift according the New Theory, which is a solution of equation (8) equals:

$$\Delta \omega_{GR} = 0.00000000004011824206173742 \text{ [s}^{-1}\text{]} \quad (13)$$

Both calculated values are within the Range of the measured gravitational RedShift by the average values of both ESA satellites in the Galileo orbit

$$\Delta \omega_{\text{Measured}} = 0.000000000040118 \pm 2.2 \cdot 10^{-15} \text{ [s}^{-1}\text{]} \quad (14)$$

In [2] a factor  $\alpha$  has been defined which presents the measured deviation  $\alpha$  between the predicted Gravitational RedShift by General Relativity and the Measured Gravitational RedShift.

$$\alpha = \Delta \omega_{\text{MEASURED}} - \Delta \omega_{\text{GR}} = (2.2 \pm 1.6) \times 10^{-5} \quad (15)$$

A comparable factor  $\alpha$  can be used to determine which theory (General Relativity or the New Theory) has the nearest approach to the experimentally measured data. Highly accurate measuring experiments are required with an accuracy higher than 16 digits beyond the decimal point.

### 3 Black Holes

#### 3.1 Black Holes without Singularities with dimensions smaller than the diameter of the Hydrogen Atom

A second fundamental solution for equation (8) describes a **Gravitational Electromagnetic Confinement (BLACK HOLE)** [1] within a radial gravitational field with acceleration  $\bar{g}$  (in radial direction). This solution represents a Black Hole, the confinement of light due to its own gravitational field, and has no singularities. This solution for equation (8) describes Black Holes, dependent of time and radius, presenting discrete spherical energy levels, within a radial gravitational field with acceleration  $\bar{g}$  (in radial direction) [14] has been represented in (16) and (17).

$$\begin{pmatrix} E_r \\ E_\theta \\ E_\varphi \end{pmatrix} = \begin{pmatrix} 0 \\ f(r) \sin(kr) \sin(\omega t) \\ -f(r) \cos(kr) \cos(\omega t) \end{pmatrix} \quad \begin{pmatrix} H_r \\ H_\theta \\ H_\varphi \end{pmatrix} = \sqrt{\frac{\epsilon}{\mu}} \begin{pmatrix} 0 \\ -f(r) \sin(kr) \cos(\omega t) \\ -f(r) \cos(kr) \sin(\omega t) \end{pmatrix} \quad \bar{g} = \begin{pmatrix} \frac{G_1}{4\pi r^2} \\ 0 \\ 0 \end{pmatrix} \quad (16)$$

$$w_{em} = \left( \frac{\mu_0}{2} (\bar{m} \cdot \bar{m}) + \frac{\epsilon_0}{2} (\bar{e} \cdot \bar{e}) \right) =$$

$$f(r)^2 \left( (\sin(kr) \sin(\omega t))^2 + (\cos(kr) \cos(\omega t))^2 + \frac{\epsilon}{\mu} (\sin(kr) \cos(\omega t))^2 + (\cos(kr) \sin(\omega t))^2 \right)$$

In which the radial function  $f(r)$  equals:

$$f[r] = K e^{-\frac{G M_{BH} \epsilon_0 \mu_0}{8\pi r}} \quad (17)$$

$G$  represents the Gravitational constant and  $M$  represents the total confined electromagnetic mass of the BLACK HOLE. Equation (16) presents a Standing (Confined) Electromagnetic Field Configuration with a phase shift of 90 degrees between the electric field and the magnetic field with the corresponding Nodes and AntiNodes. [13]. The solution has been calculated according [Newton's Shell Theorem](#).

Assuming a constant speed of light “ $c$ ” and Planck's constant  $\hbar$  within the BLACK HOLE, the radius “ $R$ ” (with  $n = 1, 2, 3, 4, \dots$ ) of the BLACK HOLE with the energy of a proton, according  $W = m_{proton} c^2$ , would be:  $1.5009211 \times 10^{-10}$  [J].



$$R_{\text{GEON}} = n \lambda = n \left( \frac{c}{f} \right) = n \left( \frac{c}{W} \right) \hbar = 7.1865 \cdot 10^{-26} \left( \frac{n}{W} \right) \quad (18)$$

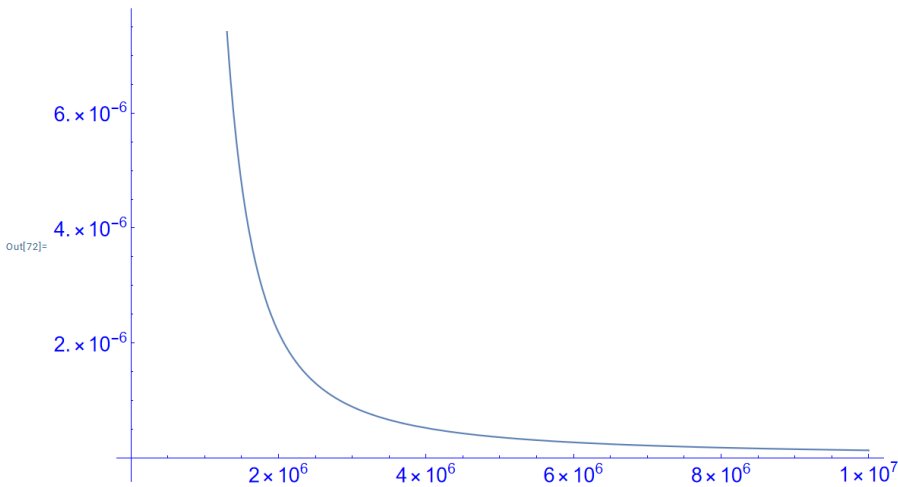
$$R_{\text{GEON}} = n \cdot 3.82 \cdot 10^{-12} \text{ [m]}$$

Black Holes are varying from atomic dimensions with dimensions of  $10^{-27}$  [kg], Page 39 [33] until Black Holes with dimensions of  $10^{40}$  [kg], Page 67 [34]. At these dimensions Black Holes turn into Dark Matter. The fundamental boundary condition for the confinement of Electromagnetic radiation (BLACK HOLES) is that the energy flow (Poynting vector)  $\vec{S} = \vec{E} \times \vec{H}$  equals zero at the surface of the confinement. This is possible at every “*90 degrees Phase Shift Surface*” (*Sphere*) between the Electric Field and the Magnetic Field.

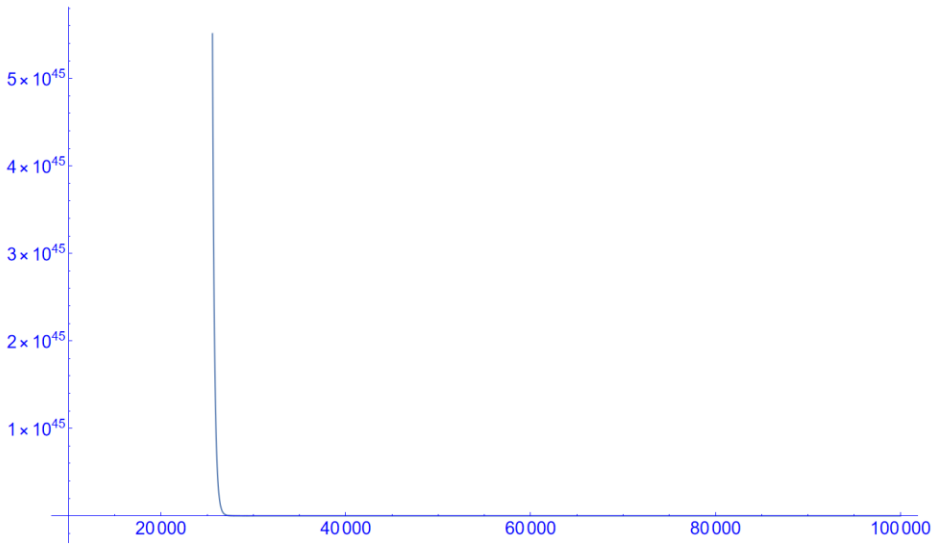
### 3.1 Black Holes with a Singular point and Large dimensions

Fig 1 represents a Black Hole with a mass of  $10^{35}$  [kg] and a radius of about 25 [km] controlled by a different mathematical solution for equation (8). The radius of the Black Hole equals about 25 [km] which has been controlled by a different mathematical solution (19) for equation (8).

$$f[r] = K e^{\left( \frac{G M_{\text{BH}} \epsilon_0 \mu_0}{8 \pi r} - \log[r] \right)} \quad [\text{J} / \text{m}^3] \quad (19)$$



**Fig. 1 The Energy Density [ J/ m<sup>3</sup>] as a function of the Radius R = max 10<sup>7</sup> [m] of the Black Hole.**



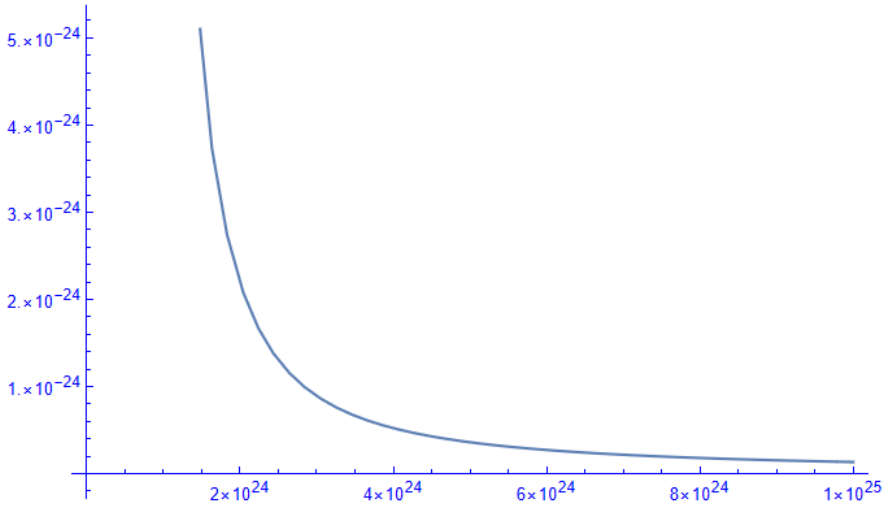
**Fig. 2 The Energy Density [ J/ m<sup>3</sup>] as a function of the Radius R = max 10<sup>5</sup> [m]**

Figure 1 and Figure 2 demonstrate the large effect of “Gravitational Intensity Shift” and “Gravitational RedShift” at the distance of 25 [km]. Over a distance of 10.000 [km] the intensity of the emitted light of the Black Hole with a mass of 10<sup>35</sup> [kg] falls back with a factor of 10<sup>-51</sup>. Also the frequency of the emitted light of the Black Hole falls back with a factor 10<sup>-51</sup>. Emitted light in the visible spectrum of 10<sup>14</sup> [Hz] falls back to a frequency of 10<sup>-37</sup> [Hz]. These extreme low frequencies with extreme low intensities have never been measured which has result in the name “Black Hole” for the phenomenon of “Gravitational Intensity Shift” and “Gravitational RedShift” for a large mass. It follows from equation (8) and the solutions (10) and (11) that the speed of light does not change inside and around Black Hole. Only the direction of the propagation of light can change due to a gravitational field.

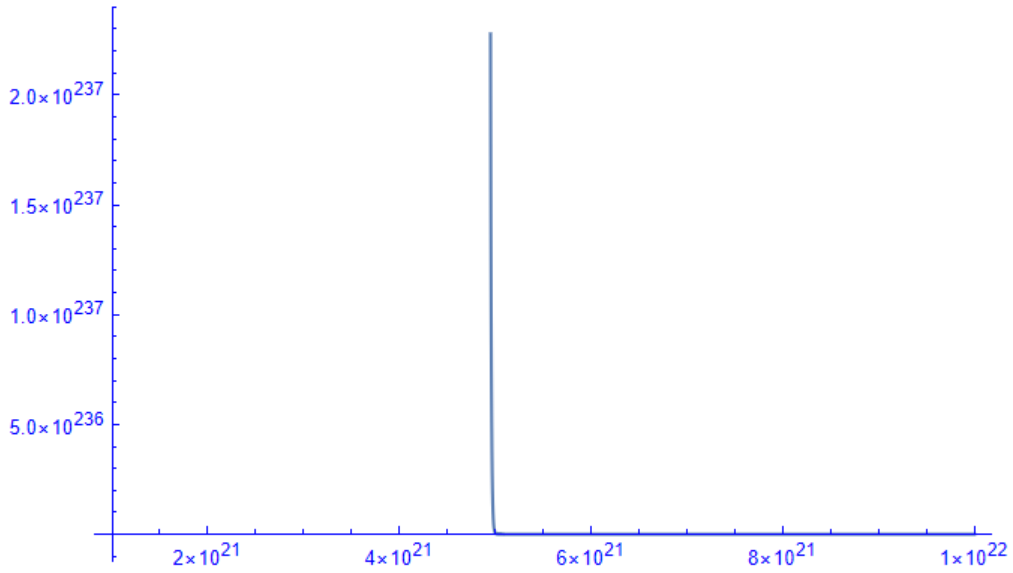
### 3.2 Dark Matter in the Universe controlled by “Gravitational Shielding”

Fig 3 represents Dark Matter with a total mass of  $10^{53}$  [kg] and a radius of about 10 times the size of the Milky Way Galaxy. The radius of the dark mass equals  $5 \cdot 10^{21}$  [m] which has been controlled by a different mathematical solution (20) for equation (8).

$$f[r] = K e^{\left( \frac{G M_{BH} \epsilon_0 \mu_0}{8 \pi r} - \log[r] \right)} \quad [J / m^3] \quad (20)$$



**Fig. 3 The Energy Density [ J/ m³] as a function of the Radius R = max  $10^{25}$  [m] of the Dark Matter.**



**Fig. 4 The Energy Density [ J/ m<sup>3</sup>] of the Dark Matter as a function of the Radius R = max 10<sup>22</sup> [m]**

Figure 3 and Figure 4 demonstrate the large effect of “Gravitational Intensity Shift” and “Gravitational RedShift” at the distance of  $5 \cdot 10^{21}$  [m] which is 10 times the radius of the Milky Way Galaxy. Over the distance of  $5 \cdot 10^{21}$  [m] the intensity of the emitted light of the Dark Matter with a mass of  $10^{53}$  [kg] falls back with a factor of  $10^{-261}$ . Also the frequency of the emitted light of the Black Hole falls back with a factor  $10^{-261}$ . Emitted light in the visible spectrum of  $10^{14}$  [Hz] falls back to a frequency of  $10^{-247}$  [Hz]. These extreme low frequencies with extreme low intensities have never been measured which has result in the name “Dark Matter” for the phenomenon of “Gravitational Intensity Shift” and “Gravitational RedShift” for an extreme large mass. It follows from equation (8) and the solutions (10) and (11) that the speed of light does not change inside and around the Dark Mass. Only the direction of the propagation of light can change due to the gravitational field of the Dark Mass.

#### 4 The relationship between Black Holes and Quantum Physics

Introducing the Quantum Vector Function  $\bar{\phi}$  ,

$$\bar{\phi} = \sqrt{\frac{\mu}{2}} \left( \bar{H} + i \frac{\bar{E}}{c} \right) \quad (21)$$

Substituting (21) in (16) results in the quantum presentation for the BLACK HOLE:

$$\overline{\Phi(r, \theta, \varphi)} = \sqrt{\frac{\mu}{2}} \left( \bar{H} + i \frac{\bar{E}}{c} \right) f(r) \begin{pmatrix} \Phi_r \\ \Phi_\theta \\ \Phi_\varphi \end{pmatrix} \quad (22)$$

$$\overline{\Phi(r, \theta, \varphi)} = K \sqrt{\frac{\varepsilon}{\mu}} e^{-\frac{G I \varepsilon_0 \mu_0}{8 \pi r}} \begin{pmatrix} 0 & 0 & 0 \\ 0 & -\sin(k r) & \sin(k r) \\ 0 & -i \cos(k r) & i \cos(k r) \end{pmatrix} \begin{Bmatrix} 0 \\ \cos(\omega t) \\ i \sin(\omega t) \end{Bmatrix}$$

With “K” a constant value dependend of the mass of the BLACK HOLE. The Dot product between the unit vector and the Quantum Vector Function  $\bar{\phi}$  represents the quantum mechanical probability function  $\Psi[r, t]$  which is a fundamental solution of the Schrödinger Wave Equation.

$$\overline{\Phi(r, \theta, \varphi)} = K \sqrt{\frac{\varepsilon}{\mu}} e^{-\frac{G l \varepsilon_0 \mu_0}{8 \pi r}} \begin{pmatrix} 0 & 0 & 0 \\ 0 & -\sin(k r) & \sin(k r) \\ 0 & -i \cos(k r) & i \cos(k r) \end{pmatrix} \begin{Bmatrix} 0 \\ \cos(\omega t) \\ i \sin(\omega t) \end{Bmatrix} \quad (23)$$

$$\Psi(r, t) = \begin{Bmatrix} 1 & 1 & 1 \end{Bmatrix} \begin{Bmatrix} 0 \\ \cos(\omega t) \\ i \sin(\omega t) \end{Bmatrix} K \sqrt{\frac{\varepsilon}{\mu}} e^{-\frac{G l \varepsilon_0 \mu_0}{8 \pi r}} = K \sqrt{\frac{\varepsilon}{\mu}} e^{-\frac{G l \varepsilon_0 \mu_0}{8 \pi r}} e^{i \omega t}$$

The Scalar function  $\Psi[r, t]$  represents a fundamental solution of the Quantum Mechanical Schrödinger wave equation. [36, 37]

#### 4.1 Black Holes with Discrete Spherical Energy Levels at Sub-Atomic dimensions

In order to effectively confine Electromagnetic Energy, a critical requirement is that the Poynting vector reaches a value of zero at the surface of the spherical confinement. Creating this confinement within a sphere necessitates the presence of a standing electromagnetic wave pattern, characterized by concentric spheres. Each of these spheres establishes an antinodal plane for either the Electric Field (E) or the Magnetic Field (B), with the radius distance between each sphere precisely equal to half the wavelength of the overall confinement.

Within this setup, a constant denoted as "k" is introduced, defined as  $k = n\pi/\lambda$ , where "n" represents a natural number (1, 2, 3, 4, ...) and  $\lambda$  signifies the wavelength of the radiation. This equation elucidates the structured connection between the wavelength, the constant k, and the natural number n within the sphere of electromagnetic confinement in a spherical system.

#### 4.1.1 Time and Radius dependent Black Holes with discrete Energy Levels. The confinements of Electromagnetic Radiation within spherical Regions.

Every concentric sphere represents an anti-nodal surface for the Electric Field (E) or the Magnetic Field (H). The Poynting Vector:  $\vec{S} = \vec{E} \times \vec{H}$  at this spherical surface equals zero at any time and at any location at this sphere. The Electromagnetic Energy remains always within this sphere and the next concentric sphere. The concentric spheres have a difference in radius of one half wavelength of the electromagnetic radiation within the confinement and a different discrete energy level. Every concentric sphere represents an anti-nodal surface of the electric field or the magnetic field.

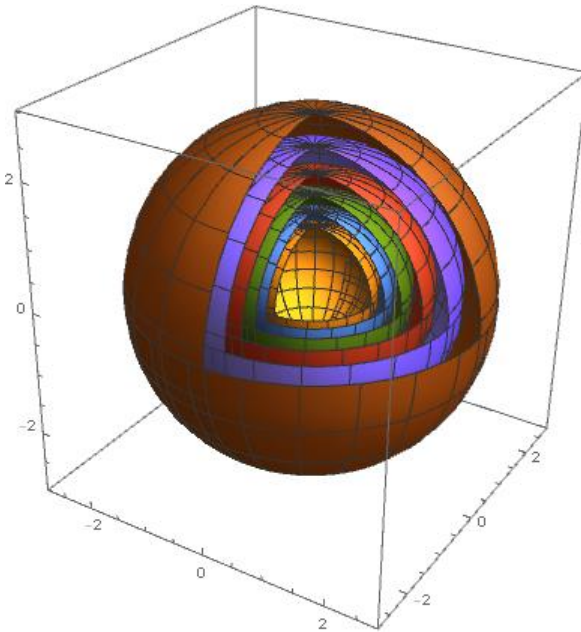


**Fig. 5 Nodal and Antinodal Spheres for Standing (Confined) Spherical Electromagnetic waves with a 90 degrees phase shift between the Electric field and the Magnetic field. Equation (23)**

Figure 5 illustrates the spatial distribution of nodal and antinodal spheres concerning stationary, confined spherical electromagnetic waves characterized by a distinctive 90-degree phase disparity between the electric and magnetic fields. This configuration is delineated by Equation (23) which encapsulates the nuanced interplay between these fundamental electromagnetic components within a three-dimensional framework.



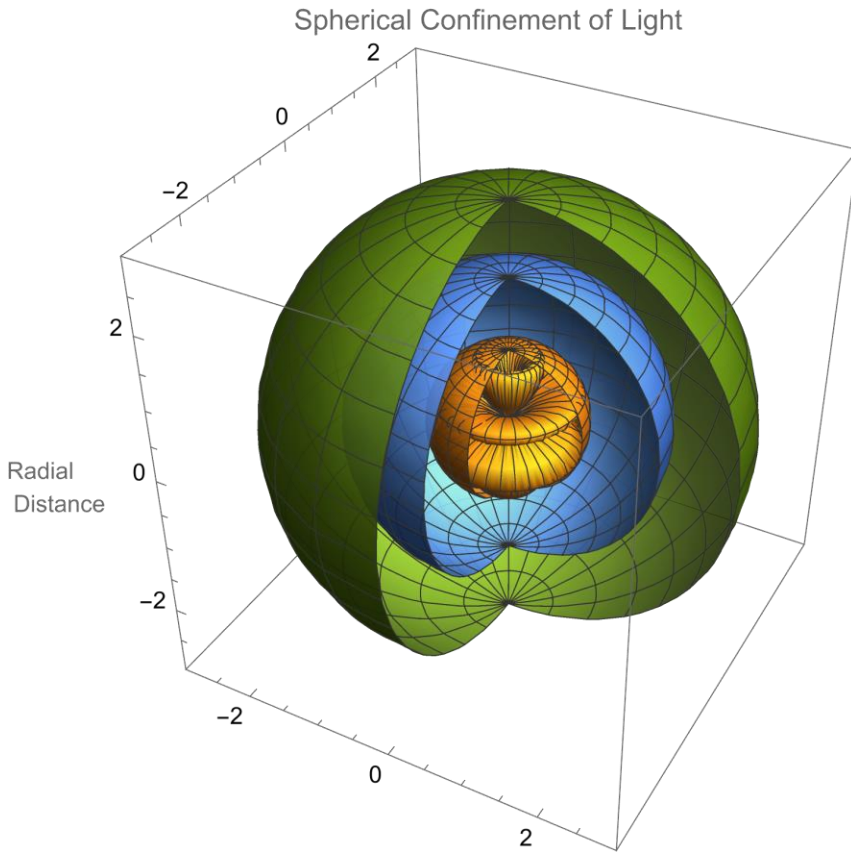


**Fig. 6 Nodal- and Anti-nodal Spheres ( $k = 3$ ) for Standing (Confined) Spherical Electromagnetic waves with a 90 degrees phase shift between the Electric field and the Magnetic field. Equation (23)**

Figure 6 depicts the intricate nodal and anti-nodal spheres, emphasizing the scenario of standing, confined spherical electromagnetic waves where the wave number  $k$  is set at 3. This visualization captures the unique 90-degree phase offset prevailing between the electric and magnetic fields. Equation (23) serves as the key mathematical representation encapsulating this phenomenon, further elucidating the interplay and characteristics of these electromagnetic waves within a specific spatial context.

Equation (24) describes a Time and Radius dependent BLACK HOLE.

$$\begin{aligned}\bar{\mathbf{E}} = & \mathbf{K} e^{-\frac{G1\epsilon_0\mu_0}{8\pi r}} \begin{pmatrix} 0 \\ \text{Sin}[k r] \text{Sin}[\omega t] \\ -\text{Cos}[k r] \text{Cos}[\omega t] \end{pmatrix} \\ \bar{\mathbf{H}} = & \mathbf{K} e^{-\frac{G1\epsilon_0\mu_0}{8\pi r}} \sqrt{\frac{\epsilon_0}{\mu_0}} \begin{pmatrix} 0 \\ \text{Sin}[k r] \text{Cos}[\omega t] \\ -\text{Cos}[k r] \text{Sin}[\omega t] \end{pmatrix}\end{aligned}\tag{24}$$

Equation (20) represents by the function  $\text{Sin}[k r]$  ( $k = 1,2,3,4,\dots$ ) the confinement of electromagnetic radiation between two concentric spheres.  $\mathbf{K}$  represents the amplitude of the Electric/ Magnetic Field Intensty. [14]

### 4.1.2 Time and Polar Angle dependent Black Holes

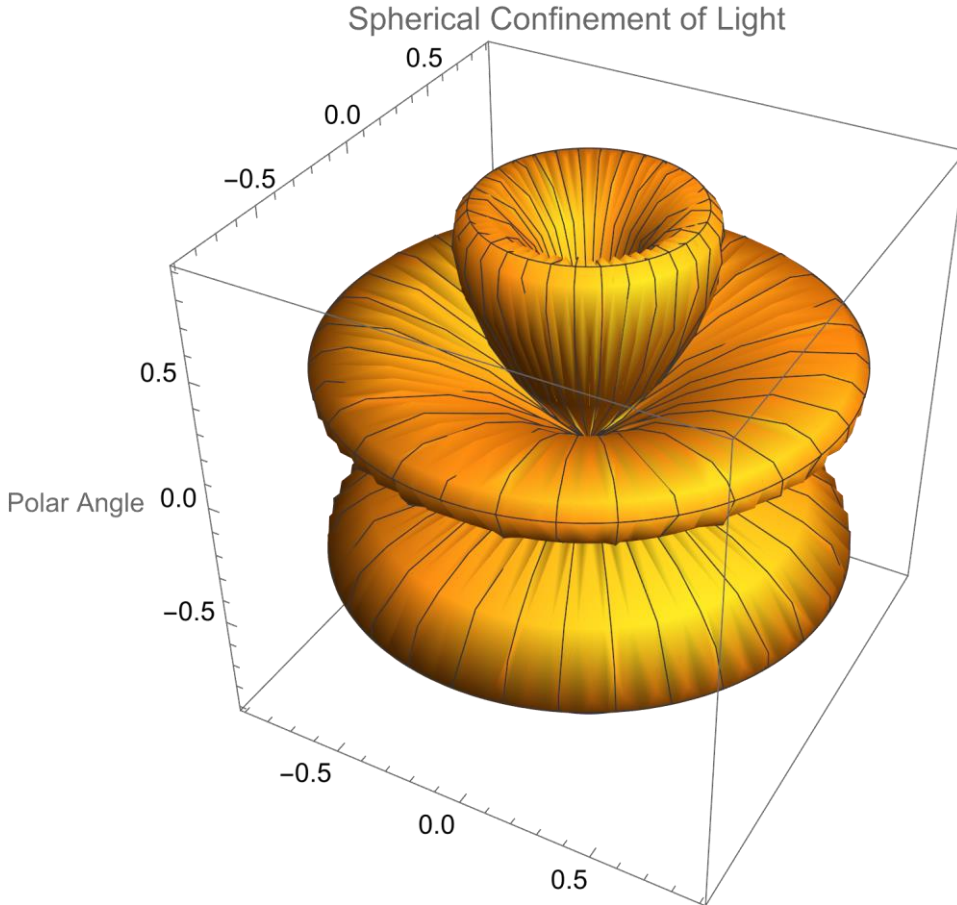


**Fig. 7 Nodal- and Antinodal Polar Angle Regions ( $m = 3$ ) for Standing (Confined) Spherical Electromagnetic waves with a 90 degrees phase shift between the Electric field and the Magnetic field. Equation (15)**

In the realm of time and polar angle-dependent black holes, Section 4.1.2 explores the intricate dynamics associated with these celestial entities. Figure 7 offers a detailed insight into the nodal and antinodal regions across the polar angle, particularly emphasizing the case where the azimuthal quantum number  $m$  is defined as 3. These findings shed light on the behavior of standing, confined spherical electromagnetic waves featuring a distinct 90-degree phase discrepancy between the electric and magnetic fields, as encapsulated by Equation (25).

Equation (25) describes a Time and “Polar Angle” dependent BLACK HOLE

$$\bar{E} = K e^{-\frac{G1\epsilon_0\mu_0}{8\pi r}} \begin{pmatrix} 0 \\ \sin[m \theta] \sin[\omega t] \\ \sin[m \theta] \cos[\omega t] \end{pmatrix} \quad (25)$$

$$\bar{H} = K e^{-\frac{G1\epsilon_0\mu_0}{8\pi r}} \sqrt{\frac{\epsilon_0}{\mu_0}} \begin{pmatrix} 0 \\ \sin[m \theta] \cos[\omega t] \\ -\sin[m \theta] \sin[\omega t] \end{pmatrix}$$

Equation (25) represents by the function  $\sin[m \theta]$  ( $m = 1, 2, 3, 4, \dots$ ) the confinement of electromagnetic radiation between two Polar Angular Regions [15].

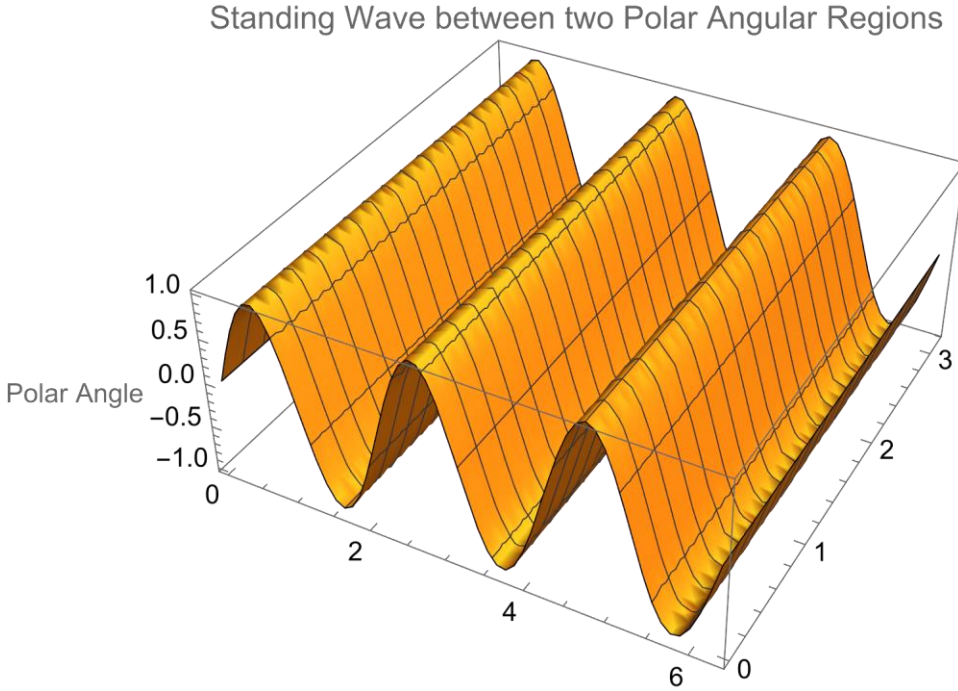


**Fig. 8 Nodal- and Antinodal Polar Angle Regions ( $m = 3$ ) for Standing (Confined) Electromagnetic waves with a 90 degrees phase shift between the Electric field and the Magnetic field. Equation (25)**

Figure 8 illustrates the regions of nodal and antinodal behavior with respect to the polar angle, specifically focusing on cases where the azimuthal quantum number  $m$  is set to 3. This visualization pertains to standing, confined electromagnetic waves displaying a significant 90-degree phase differential between the electric and magnetic fields. The underlying dynamics are succinctly captured by Equation (15), providing a formal representation of these intriguing wave patterns.

#### 4.1.3 Time and Azimuthal Angular dependent Black Holes

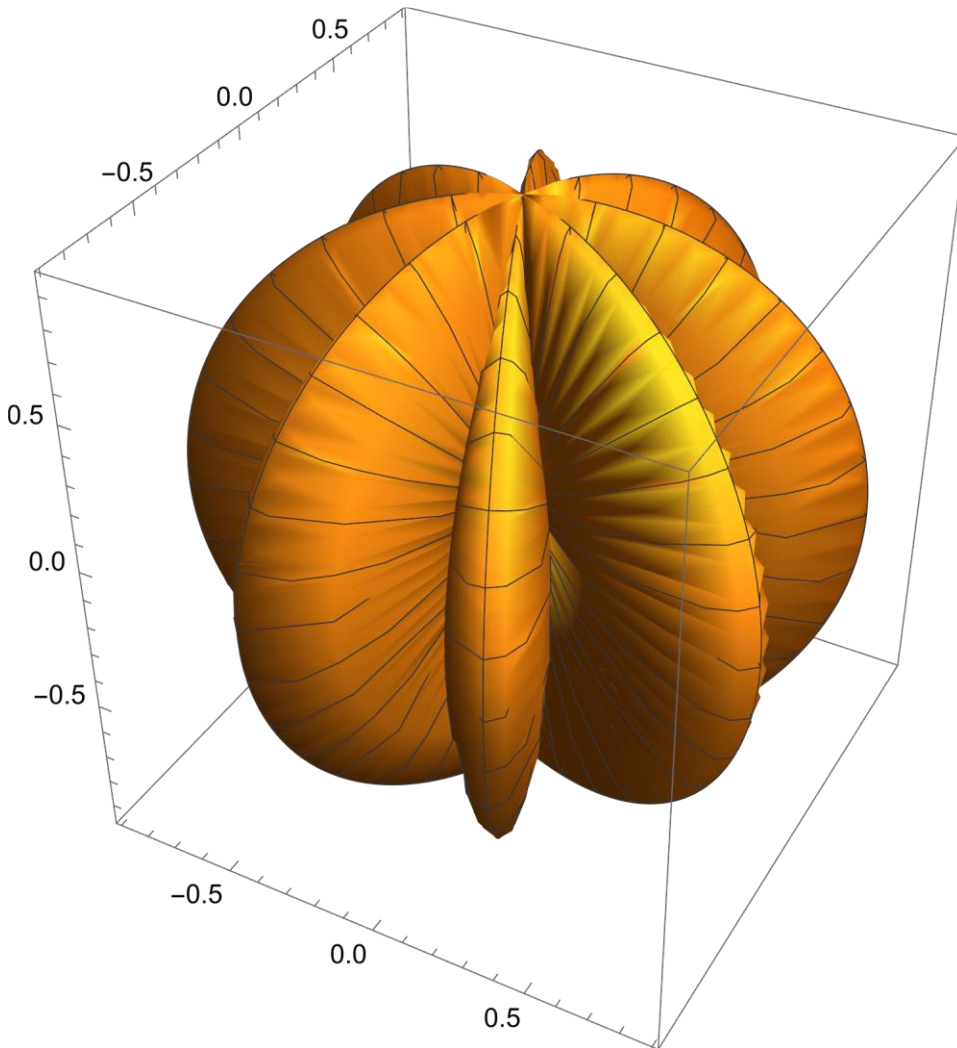


**Fig. 9 Nodal- and Antinodal Azimuthal Angular Regions ( $n = 3$ ) for Standing (Confined) Electromagnetic waves with a 90 degrees phase shift between the Electric field and the Magnetic field. Equation (26)**

Fig. 9 Nodal- and Anti-nodal Azimuthal Angular Regions ( $n = 3$ ) for Standing (Confined) Electromagnetic waves with a 90 degrees phase shift between the Electric field and the Magnetic field. Equation (26). Equation (26) describes a Time and “Polar Angle” dependent BLACK HOLE

$$\bar{E} = K e^{-\frac{G1\epsilon_0\mu_0}{8\pi r}} \begin{pmatrix} 0 \\ \cos[n \varphi] \sin[\omega t] \\ \cos[n \varphi] \cos[\omega t] \end{pmatrix} \quad (26)$$

$$\bar{H} = K e^{-\frac{G1\epsilon_0\mu_0}{8\pi r}} \sqrt{\frac{\epsilon_0}{\mu_0}} \begin{pmatrix} 0 \\ \cos[n \varphi] \cos[\omega t] \\ -\cos[n \varphi] \sin[\omega t] \end{pmatrix}$$

The function denoted by Equation (26), where  $n$  ranges over integers ( $n = 1, 2, 3, \dots$ ), encapsulates the confinement of electromagnetic radiation within two distinct Azimuthal Angular Regions, as referenced by [16].

#### 4.1.4 Time, Polar- and Azimuthal Angular dependent Black Holes

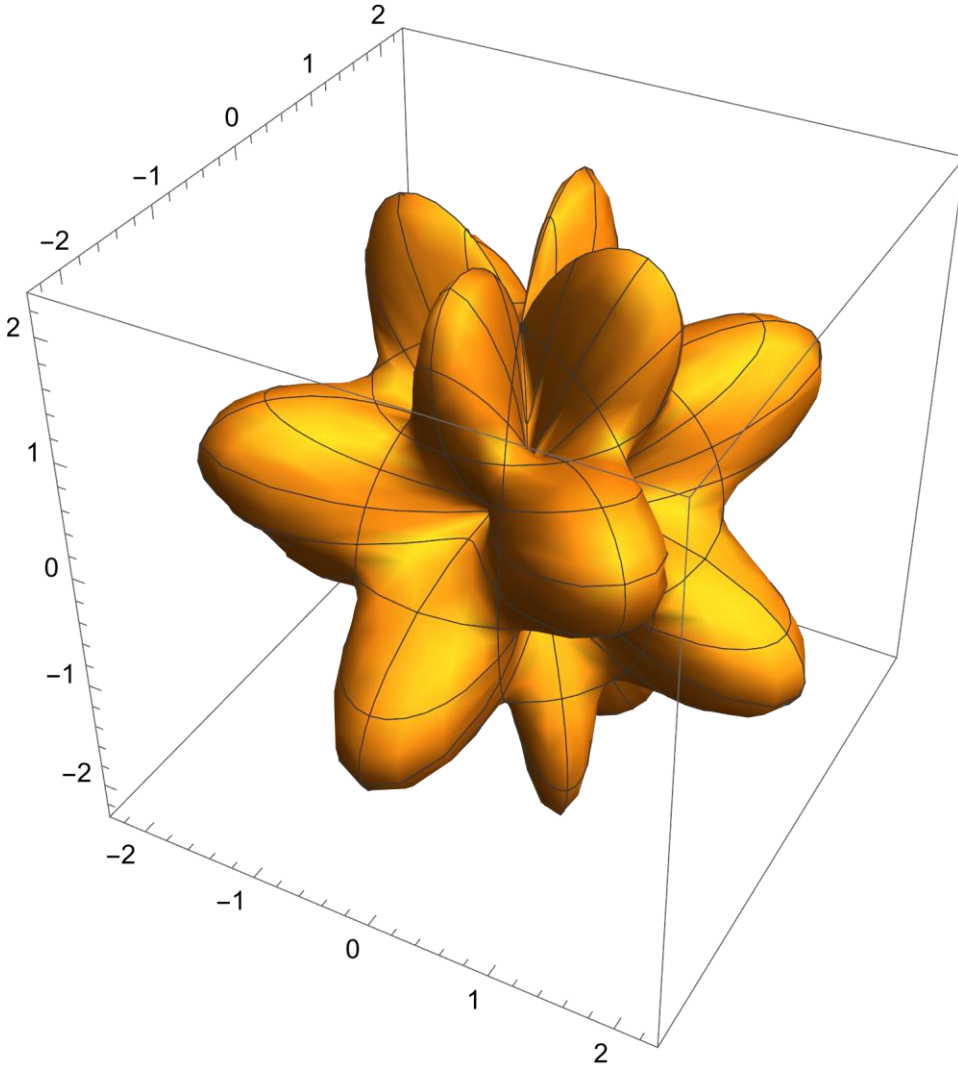


**Fig. 10 Nodal- and Anti-nodal Polar Angular and Azimuthal Angular Regions ( $n = 4$  and  $m = 4$ ) for Standing (Confined) Electromagnetic waves with a 90 degrees phase shift between the Electric field and the Magnetic field. Equation (27)**

Figure 10 showcases the delineation of nodal and anti-nodal regions pertaining to both polar and azimuthal angular domains, specifically when  $n$  is set to 4 and  $m$  is set to 4. This visualization sheds light on the intricate behavior of standing, confined electromagnetic waves characterized by a distinct 90-degree phase difference between the electric and magnetic fields. The mathematical framework governing

these phenomena is encapsulated by Equation (27), providing a formal expression of these electromagnetic wave patterns within the specified angular regions.

Equation (27) describes a Time “Azimuthal Angle” and “Polar Angle” dependent BLACK HOLE

$$\begin{aligned} \bar{E} = & K e^{-\frac{G1\epsilon_0\mu_0}{8\pi r}} \begin{pmatrix} 0 \\ \text{Cos}[n \varphi] \text{Sin}[m \theta] \text{Sin}[\omega t] \\ \text{Cos}[n \varphi] \text{Sin}[m \theta] \text{Cos}[\omega t] \end{pmatrix} \\ & (27) \\ \bar{H} = & K e^{-\frac{G1\epsilon_0\mu_0}{8\pi r}} \sqrt{\frac{\epsilon_0}{\mu_0}} \begin{pmatrix} 0 \\ -\text{Cos}[n \varphi] \text{Sin}[m \theta] \text{Cos}[\omega t] \\ \text{Cos}[n \varphi] \text{Sin}[m \theta] \text{Sin}[\omega t] \end{pmatrix} \end{aligned}$$

Equation (27) represents by the function  $\text{Cos}[n \varphi]$  ( $n = 1, 2, 3, 4, \dots$ ) and  $\text{Sin}[m \theta]$  ( $m = 1, 2, 3, 4, \dots$ ) the confinement of electromagnetic radiation between two Azimuthal Angular Regions and two Polar Angulars Regions [17].



#### 4.1.5 Spherical Confinement of Light between two Concentric Spheres within Black Holes

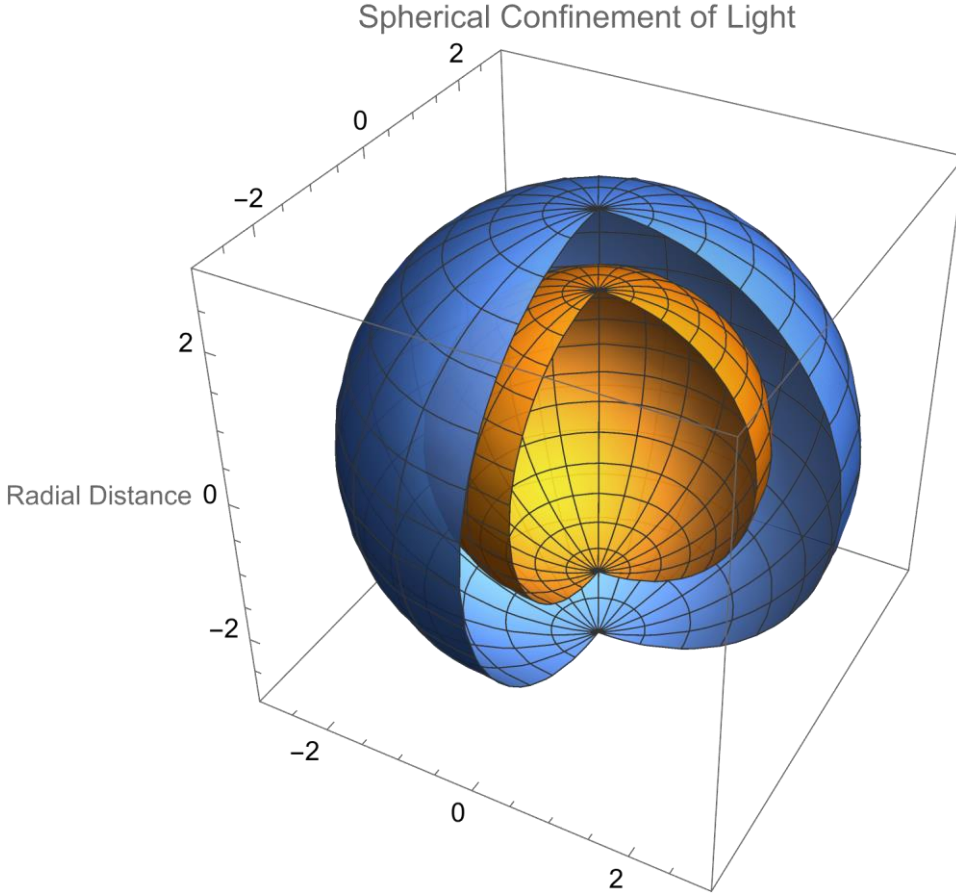


**Fig.11 Nodal- and Antinodal Regions for Standing (Confined) Electromagnetic waves with a 90 degrees phase shift between the Electric field and the Magnetic field. Equation (14)**

Figure 11 illustrates the nodal and antinodal regions associated with standing, confined electromagnetic waves featuring a 90-degree phase differential between the electric and magnetic fields. The intricacies of this wave behavior are represented mathematically by Equation (14), offering a formal description of the electromagnetic field dynamics within this context.

Equation (28) captures the phenomenon of the reflection of Confined Electromagnetic Energy within the confines of a Black Hole, delineated between two concentric spheres. In this scenario, the speed of light, which is contingent upon the

variable "r" representing the radial distance, undergoes a change in direction commensurate with the frequency of the confined light, or Electromagnetic Radiation.

Remarkably, a Black Hole possesses the capacity to undergo a process of splitting into two distinct Black Holes characterized by differing radii. During this transformation, the original Black Hole transitions to a lower energy level, akin to an atom descending to a lower energy state. The resultant new Black Holes formed as a consequence of this splitting represent the disparity in energy levels, resembling the analogous behavior of an atom transitioning between energy levels within its atomic structure.

$$\begin{aligned}\bar{E} &= K e^{-\frac{G1\epsilon_0\mu_0}{8\pi r}} f \left[ t - \frac{\sqrt{\epsilon_0 \mu_0} \cos[2 k r]}{2 k} \right] \begin{pmatrix} 0 \\ \sin[k r] \sin[\omega t] \\ -\cos[k r] \cos[\omega t] \end{pmatrix} \\ \bar{H} &= K e^{-\frac{G1\epsilon_0\mu_0}{8\pi r}} f \left[ t - \frac{\sqrt{\epsilon_0 \mu_0} \cos[2 k r]}{2 k} \right] \sqrt{\frac{\epsilon_0}{\mu_0}} \begin{pmatrix} 0 \\ -\sin[k r] \cos[\omega t] \\ -\cos[k r] \sin[\omega t] \end{pmatrix}\end{aligned}\tag{28}$$

## Spherical Confinement of Light between two Concentric Spheres

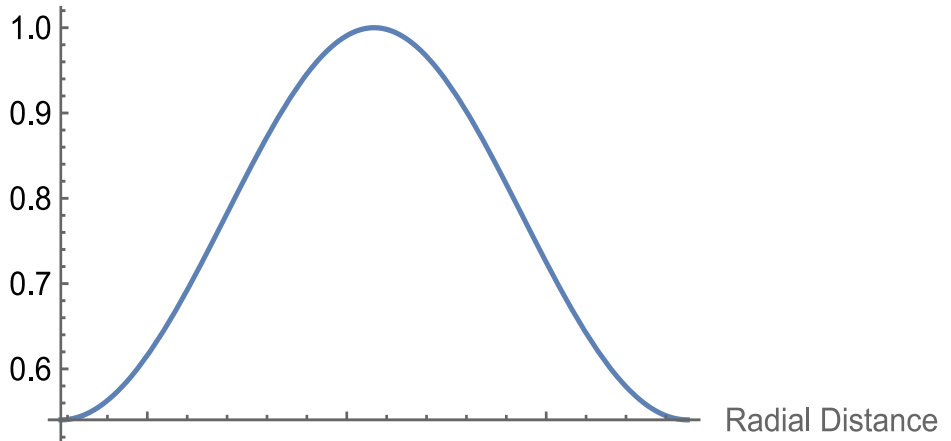


**Fig. 12 Nodal- and Antinodal Regions for Standing (Confined) Electromagnetic within two concentric spheres. Equation (18)**

Figure 12 presents a visual representation of the nodal and anti-nodal regions characterizing standing, confined electromagnetic waves enclosed within two concentric spheres. The electromagnetic field behaviors within this configuration are mathematically defined by Equation (18), offering a precise formulation of the wave dynamics within the specified spatial constraints.

### 4.2 5

### 4.3 Universal Equilibrium in the “Concept of Quantum Mechanical Probability” in “The New Theory”.

The 4-dimensional notation for the divergence of the Stress-Energy Tensor (25) expresses in the 4<sup>th</sup> dimension (time dimension) the law of [Conservation of Energy](#). For an Electromagnetic Field the law for conservation of Energy has been expressed as:

$$\bar{f}^4 = \begin{pmatrix} f_4 \\ f_3 \\ f_2 \\ f_1 \end{pmatrix} = \square \cdot \bar{\bar{T}} = \begin{pmatrix} \nabla \cdot \bar{S} + \frac{\partial w}{\partial t} \\ f_3 \\ f_2 \\ f_1 \end{pmatrix} = \bar{0}^4 \quad (29)$$

From the equation for the “Conservation of Electromagnetic Energy” (38.1) the “Fundamental Equation for Confined Electromagnetic Interaction” in “The New Theory” will be derived, which equals the Relativistic Quantum Mechanical “Dirac” equation and the Schrödinger wave equation at velocities relative low compared to the speed of light.

The “Fundamental Equation for Confined Electromagnetic Interaction” in “The Proposed Theory” can be considered to be the relativistic version of the Quantum Mechanical Schrödinger wave equation, which equals the Quantum Mechanical Dirac Equation.

## 5.1 Confined Electromagnetic Energy within a 4-dimensional Equilibrium

The physical concept of quantum mechanical probability waves has been created during the famous [1927 5<sup>th</sup> Solvay Conference](#). During that period there were several circumstances which came just together and made it possible to create a unique idea of “**Material Waves**” (Solutions of Schödinger’s wave equation) being complex (partly real and partly imaginary) and describing the probability of the appearance of a physical object (elementary particle) generally indicated as “**Quantum Mechanical Probability Waves**”.

The idea of complex (probability) waves is directly related to the concept of confined ([standing](#)) waves. Characteristic for any [standing](#) acoustical wave is the fact that the Velocity and the Pressure (Electric Field and Magnetic Field in QLT) are always shifted over 90 degrees. The same principle does exist for the [standing \(confined\) electromagnetic waves](#),

For that reason every confined (standing) Electromagnetic wave can be described by a complex sum vector  $\bar{\phi}$  of the Electric Field Vector  $\bar{E}$  and the Magnetic Field Vector  $\bar{B}$  ( $\bar{E}$  has 90 degrees phase shift compared to  $\bar{B}$  ).

The vector functions  $\bar{\phi}$  and the complex conjugated vector function  $\bar{\phi}^*$  will be written as:

$$\bar{\phi} = \frac{1}{\sqrt{2}\mu} \left( \bar{B} + i \frac{\bar{E}}{c} \right) \quad (30)$$

$\bar{B}$  equals the magnetic induction,  $\bar{E}$  the electric field intensity ( $\bar{E}$  has + 90 degrees phase shift compared to  $\bar{B}$  ) and  $c$  the speed of light.

The complex conjugated vector function  $\bar{\phi}^*$  equals:

$$\bar{\phi}^* = \frac{1}{\sqrt{2}\mu} \left( \bar{B} - i \frac{\bar{E}}{c} \right) \quad (31)$$

The dot product equals the electromagnetic energy density  $w$ :

$$\bar{\phi} \cdot \bar{\phi}^* = \frac{1}{2\mu} \left( \bar{\mathbf{B}} + i \frac{\bar{\mathbf{E}}}{c} \right) \cdot \left( \bar{\mathbf{B}} - i \frac{\bar{\mathbf{E}}}{c} \right) = \frac{1}{2} \mu H^2 + \frac{1}{2} \varepsilon E^2 = w \quad (32)$$

Using Einstein's equation  $W = m c^2$ , the dot product equals the electromagnetic mass density  $w$ :

$$\bar{\phi} \cdot \bar{\phi}^* \frac{1}{c^2} = \frac{\varepsilon}{2} \left( \bar{\mathbf{B}} + i \frac{\bar{\mathbf{E}}}{c} \right) \cdot \left( \bar{\mathbf{B}} - i \frac{\bar{\mathbf{E}}}{c} \right) = \frac{1}{2} \varepsilon \mu^2 H^2 + \frac{1}{2} \varepsilon^2 E^2 = \rho \text{ [kg/m}^3\text{]} \quad (33)$$

The cross product is proportional to the Poynting vector [\(Ref. 3, page 202, equation 15\)](#).

$$\bar{\phi} \times \bar{\phi}^* = \frac{1}{2\mu} \left( \bar{\mathbf{B}} + i \frac{\bar{\mathbf{E}}}{c} \right) \times \left( \bar{\mathbf{B}} - i \frac{\bar{\mathbf{E}}}{c} \right) = i \sqrt{\varepsilon \mu} \bar{\mathbf{E}} \times \bar{\mathbf{H}} = i \sqrt{\varepsilon \mu} \bar{\mathbf{S}} \quad (34)$$

This article presents a new “Gravitational-Electromagnetic Equation” describing Electromagnetic Field Configurations which are simultaneously the Mathematical Solutions for the Scalar Quantum Mechanical “Schrodinger Wave Equation” and more exactly the Mathematical Solutions for the Tensor representation of the “Relativistic Quantum Mechanical Dirac Equation” (41).

The 4-dimensional divergence of the sum of the Electromagnetic Stress-Energy tensor expresses the 4-dimensional Force-Density vector (expressed in  $[\text{N/m}^3]$  in the 3 spatial coordinates) as the result of Electro-Magnetic-Gravitational interaction.

$$f^\mu = \partial_\nu T^{\mu\nu} = 0 \quad (35)$$

In vector notation the 4-dimensional Force-Density vector can be written as:

$$\bar{f}^4 = \begin{pmatrix} f_4 \\ f_3 \\ f_2 \\ f_1 \end{pmatrix} = \square \cdot \bar{\mathbf{T}} = 0 \quad (36)$$

The fundamental boundary condition for this alternative approach to gravity is the requirement that the Force 4 vector equals zero in the 4 dimensions, expressing a universal 4-dimensional equilibrium:

The 3 spatial components of the Force-Density vector, as a result of Electro-Magnetic-Gravitational interaction can be written as:

Substituting the electromagnetic values for the electric field intensity “E” and the magnetic field intensity “H” in (36) results in the 4-dimensional representation of the Electro-Magnetic-Gravitational Fields Equation (37):

$$\begin{aligned}
 & \text{Energy-Time Domain} \\
 (f_4) \quad & \Leftrightarrow \nabla \cdot (\bar{\mathbf{E}} \times \bar{\mathbf{H}}) + \frac{1}{2} \frac{\partial \left( \epsilon_0 (\bar{\mathbf{E}} \cdot \bar{\mathbf{E}}) + \mu_0 (\bar{\mathbf{H}} \cdot \bar{\mathbf{H}}) \right)}{\partial t} = 0 \\
 & \text{3-Dimensional Space Domain} \tag{37} \\
 \begin{pmatrix} f_3 \\ f_2 \\ f_1 \end{pmatrix} \quad & \Leftrightarrow -\frac{1}{c^2} \frac{\partial (\bar{\mathbf{E}} \times \bar{\mathbf{H}})}{\partial t} + \epsilon_0 \bar{\mathbf{E}} (\nabla \cdot \bar{\mathbf{E}}) - \epsilon_0 \bar{\mathbf{E}} \times (\nabla \times \bar{\mathbf{E}}) \\
 & + \mu_0 \bar{\mathbf{H}} (\nabla \cdot \bar{\mathbf{H}}) - \mu_0 \bar{\mathbf{H}} \times (\nabla \times \bar{\mathbf{H}}) = \bar{\mathbf{0}}
 \end{aligned}$$

In which  $f_1$  ,  $f_2$  ,  $f_3$ , represent the force densities in the 3 spatial dimensions and  $f_4$  represent the force density (energy flow) in the time dimension (4<sup>th</sup> dimension). Equation (37) can be written as:

$$\begin{aligned}
 & \text{Energy-Time Domain} \\
 & \text{Conservation of Energy} \\
 & \text{B-7} \\
 (f_4) \quad & \nabla \cdot \bar{\mathbf{S}} + \frac{\partial w}{\partial t} = 0 \tag{38.1} \\
 & \text{3-Dimensional Space Domain} \\
 & \tag{38} \\
 & \begin{array}{ccc} \text{B-1} & \text{B-2} & \text{B-3} \\ -\frac{1}{c^2} \frac{\partial (\bar{\mathbf{E}} \times \bar{\mathbf{H}})}{\partial t} & + \epsilon_0 \bar{\mathbf{E}} (\nabla \cdot \bar{\mathbf{E}}) & - \epsilon_0 \bar{\mathbf{E}} \times (\nabla \times \bar{\mathbf{E}}) + \\ \text{B-4} & \text{B-5} & \\ + \mu_0 \bar{\mathbf{H}} (\nabla \cdot \bar{\mathbf{H}}) & - \mu_0 \bar{\mathbf{H}} \times (\nabla \times \bar{\mathbf{H}}) & = \bar{\mathbf{0}} \end{array} \tag{38.2} \\
 \begin{pmatrix} f_3 \\ f_2 \\ f_1 \end{pmatrix}
 \end{aligned}$$

The 4<sup>th</sup> term in equation (38.1) can be written in the terms of the Poynting vector “S” and the energy density “w” representing the electromagnetic law for the conservation of energy (Newton’s second law of motion).

### 5.3 The 4-dimensional Relativistic Dirac Equation

Substituting (32) and (34) in Equation (38.1) results in The 4-Dimensional Tensor presentation for the relativistic quantum mechanical Dirac Equation (39):

$$\begin{aligned}
 (x_4) \quad & \nabla \cdot (\bar{\phi} \times \bar{\phi}^*) + \frac{i}{c} \frac{\partial \bar{\phi} \cdot \bar{\phi}^*}{\partial t} = 0 \\
 \begin{pmatrix} x_3 \\ x_2 \\ x_1 \end{pmatrix} & \frac{i}{c} \frac{\partial (\bar{\phi} \times \bar{\phi}^*)}{\partial t} - \left( \bar{\phi} \times (\nabla \times \bar{\phi}^*) + \bar{\phi}^* \times (\nabla \times \bar{\phi}) \right) + \left( \bar{\phi} (\nabla \cdot \bar{\phi}^*) + \bar{\phi}^* (\nabla \cdot \bar{\phi}) \right) = 0
 \end{aligned} \tag{39}$$

To transform the electromagnetic vector wave function  $\bar{\phi}$  into a scalar (spinor or one-dimensional matrix representation), the Pauli spin matrices  $\sigma$  and the following matrices (Ref. 3 page 213, equation 99) are introduced:

$$\bar{\alpha} = \begin{bmatrix} 0 & \sigma \\ \sigma & 0 \end{bmatrix} \quad \text{and} \quad \bar{\beta} = \begin{bmatrix} \delta_{ab} & 0 \\ 0 & -\delta_{ab} \end{bmatrix} \tag{40}$$

The Equations (6), (32) and (34) can be written in tensor presentation as the 4-Dimensional Relativistic Quantum Mechanical Dirac Equation: [3] (Equation 102, page 213)

$$(x_4) \quad \left( \frac{i m c}{h} \bar{\beta} + \bar{\alpha} \cdot \nabla \right) \psi = - \frac{1}{c} \frac{\partial \psi}{\partial t} \tag{41.1}$$

$$\begin{aligned}
 \begin{pmatrix} x_3 \\ x_2 \\ x_1 \end{pmatrix} & - \frac{1}{c^2} \frac{\partial (\bar{\mathbf{E}} \times \bar{\mathbf{H}})}{\partial t} + \varepsilon_0 \bar{\mathbf{E}} (\nabla \cdot \bar{\mathbf{E}}) - \varepsilon_0 \bar{\mathbf{E}} \times (\nabla \times \bar{\mathbf{E}}) + \\
 & + \mu_0 \bar{\mathbf{H}} (\nabla \cdot \bar{\mathbf{H}}) - \mu_0 \bar{\mathbf{H}} \times (\nabla \times \bar{\mathbf{H}}) + \gamma_0 \bar{\mathbf{g}} (\nabla \cdot \bar{\mathbf{g}}) - \gamma_0 \bar{\mathbf{g}} \times (\nabla \times \bar{\mathbf{g}}) = \bar{0}
 \end{aligned} \tag{41.2}$$



## 6. The fundamental experiment to validate the New Theory in Physics

The fundamental foundation for Einstein's Theory of General Relativity is the "Curvature of Space and Time" due to a Gravitational Field. In the "Theory of General Relativity" Gravitational RedShift has been explained by a change in time and space resulting is a change in the observed frequency shift in the spectrum of the light being emitted by far away Galaxies. The foundation for Einstein's theory of General Relativity is a constant value for the speed of light in the absence of a gravitational field.

In the "New Theory" the fundamental foundation is "Equilibrium". Equilibrium for the "5 fundamental force densities in light" in any direction at any time and at any location. The 5 fundamental forces in light are:

- 1) "Inertia Force" (Energy has always inertia according Einstein's  $E = m c^2$ )
- 2) "Electric Force"
- 3) "Magnetic Force"
- 4) "Electric Force" due to the "Lorentz Transformation" of the "Magnetic Force"
- 5) "Magnetic Force" due to the "Lorentz Transformation" of the "Electric Force"

The speed of light has been fully controlled by the perfect equilibrium between the 5 fundamental force densities in any direction at any time and at any location. For a single beam of light the perfect equilibrium between the 5 fundamental forces always results in the speed of light:

$$c = 1 / \sqrt{\epsilon \mu} \quad (42) \quad .$$

However in this experiment 3 beams of light with the same frequency and the same phase and 3 controllable (LPA) different intensities K1, K2 and K3 will cross each other in 3 orthogonal directions. This will result in different boundary conditions for the total electromagnetic radiation and will be measurable by a changing in the speed of light. In this experiment by a changing of the speed of light in the chosen z-direction. The changing of the speed of light will become visible by a change in the interference patterns of the 2 LASER beams. The original beam and the manipulated beam.

The solution for equation (8) has been calculated in Mathematica when 3 laser beams cross each other perpendicular and will cause a change in the speed of light within the intersection of the 3 crossing Laser Beams due to Electromagnetic Interaction.

According the calculations in Mathematica 11.3 at the exact “**location dependent speed of light  $c[x,y,z]$** “ there will be a perfect equilibrium between all the electromagnetic- inertia- and radiation pressure force densities at any time in any direction:

$$\frac{1}{c(x,y,z)} = h[x,y,z] = \frac{(K_2^2 x^2 - K_1 K_3 x + K_3^2 y + K_1^2 z - K_2 (K_1 y + K_3 z))}{K_1^2 + K_2^2 + K_3^2} \sqrt{\epsilon_0} \sqrt{\mu_0} \quad (43)$$

The result in equation (43) has been presented in Ref [38]. The change in the speed of light in the cross section will become visible in the interference patterns on screen 1 and screen 2 by changing the intensity of the secondary and third LASER beams by the two “[LASER Power Attenuators](#)” (indicated in blue) after passing the [beamsplitter\(s\)](#).

The diagram illustrates a quantum optics experiment setup. A red laser beam from a He-Ne LASER at the bottom passes through a 100% reflecting mirror and a series of three Non-Polarizing Beamsplitters (green diagonal lines). The beam intensity is labeled as 100% after the first beamsplitter and 50% after the second. It then enters a pink oval labeled 'Area of Electromagnetic Interaction'. After exiting, the beam passes through a third beamsplitter, with 25% of the light being reflected upwards and 25% continuing forward. The forward path includes a Laser Power Attenuator (LPA, blue vertical line) and a detector K1. The reflected path from the third beamsplitter goes through a detector K2 and another LPA. The beam then reflects off a 100% reflecting mirror and passes through a detector K3. The main path continues upwards through a fourth beamsplitter, with 25% of the light being reflected to the right and 25% continuing upwards. The rightward path includes an Adjustable Polarization Filter (blue vertical line) and a detector. The final upward path is labeled 25% and leads to Projection Screen 1. A label 'Vertical Direction' with a circle and a cross symbol is placed near the third beamsplitter. A legend at the bottom left shows a blue vertical line representing a Laser Power Attenuator (LPA).

## 6. Conclusions

Based on the assumption of the zero rest mass of photons, General Relativity describes the interaction between Gravity and Light within a 4-dimensional curvature in Space and Time due to a gravitational field. Light follows a path defined by this curved 4-dimensional Space and Time geometry.

The new theory, describes a bi-directional separation between mass and inertia for light (photons). Inertia can only exist only in the direction of propagation of the beam of light (photons) which determines the speed of light. Mass of the beam of light (photons) can only exist in the plane perpendicular to the direction of propagation (directions of confinement), which determines the deflection of a beam of light (photons) by a gravitational field in the plane perpendicular to the direction of propagation.

BLACK HOLES (Gravitational-Electromagnetic Confinements) are fundamental solutions of the relativistic quantum mechanical Dirac equation. Black Holes represent the large impact of “Gravitational Intensity Shift” and “Gravitational RedShift” due to a gravitational field. Both phenomena can maybe observed in the future with extremely sensitive observatories at extreme low frequency levels.

The new theory describes the impact of "CURL" [38] within the gravitational fields around Black Holes and the impact on Gravitational Lensing. Gravitational "CURL" (Equation 6) is an effect which cannot be explained and calculated by General Relativity

Within a 4-Dimensional Equilibrium and taking into account the inertia- and the gravitational- force densities within the electromagnetic field configurations, Gravitational Electromagnetic Confinements (BLACK HOLES at sub-atomic dimensions) are a physical reality and are solutions of the Relativistic Quantum Mechanical Dirac Equation (39, 41) and present spherical confinements with discrete separate energy levels.

To test the proposed theory with General Relativity, an experiment [2] has been required which measures the interaction between gravity and light within a well-defined gravitational field like the gravitational field of the earth. The difference between the calculation for Gravitational RedShift, within the Gravitational Field of the Earth, in “General Relativity” and “The New Theory” is smaller than  $10^{-16}$  and cannot be determined with present observation equipment (maximum accuracy of  $10^{-15}$  for GRS). Validation of both theories requires higher accuracies.

Dark Matter does exist because of “Gravitational RedShift” and Gravitational Intensity Shift”. A complete Galaxy, existing of billions bright light emitting star constellations, with a total mass of  $10^{53}$  [kg] becomes invisible for any observatory like the “James Webb Space Telescope” at the distance of  $5 \cdot 10^{21}$  [m] (which is 10 times the radius of the Milky Way Galaxy). This distance of “Gravitational Shielding” has been controlled by the mathematical solution (20) for equation (8). The gravitatonal field of these Galaxies has not been effected by the effect of “Gravitationa RedShift” and “Gravitational IntensityShift” at all.

For this reason a large percentage of the total mass in the Universe beyond te border of “Gravitational Shielding” becomes invisible for our observatories on and close around the earth. While the gravitational fields of these galaxies still has the full influence on our universe.

The results of the experiment to test the new theory and evaluate these experimatal values cannot be published yet because the many results of the experint has to be tested and controlled by a large number of scientific institutes before any important conclusion can be drawn form this experiment. The observed fluctuations in the interference patterns can have many reasons and this fundamental experiment has to be done and evaluated by scientific teams worldwide.

## 5.1 Data Availability

All Data and Calculations have been published at:

<https://quantumlight.science/>

## References

- [1] Wheeler; John Archibald; GEONs, Physical Review Journals Archive, 97, 511, Issue 2, pages 511-526, Published 15 January 1955, Publisher: American Physical Society, [DOI: 10.1103/PhysRev.97.511](https://doi.org/10.1103/PhysRev.97.511):
- [2] Sven Herrmann, Felix Finke, Martin Lülfi, Olga Kichakova, Dirk Puetzfeld, Daniela Knickmann, Meike List, Benny Rievers, Gabriele Giorgi, Christoph Günther, Hansjörg Dittus; Test of the Gravitational Redshift with Galileo Satellites in an Eccentric Orbit ;Phys. Rev. Lett. **121**, 231102 – Published 4 December 2018; Gravitational Redshift Test Using Eccentric Galileo Satellites, [DOI: 10.1103/PhysRevLett.121.231102](https://doi.org/10.1103/PhysRevLett.121.231102)
- [3] Vegt Wim; A Continuous Model of Matter based on AEONs, Physics Essays, Volume 8, Number 2, 1995, [DOI: 10.31219/osf.io/ra7ng](https://doi.org/10.31219/osf.io/ra7ng)
- [4] Vegt Wim; Mathematical Solutions for the Propagation of Light in Quantum Light Theory, Calculations in Mathematica 13.1: [https://community.wolfram.com/groups/-/m/t/2576692?p\\_p\\_auth=mTldHX3v](https://community.wolfram.com/groups/-/m/t/2576692?p_p_auth=mTldHX3v)
- [5] Vegt Wim; Gravitational RedShift between two Atomic Clocks, Calculations in Mathematica 13.1: [https://community.wolfram.com/groups/-/m/t/2622560?p\\_p\\_auth=EC8QO0Xz](https://community.wolfram.com/groups/-/m/t/2622560?p_p_auth=EC8QO0Xz)
- [6] Vegt Wim; Propagation of Light within a Gravitational Field in Quantum Light Theory, Calculation in Mathematica 13.1: [https://community.wolfram.com/groups/-/m/t/2576537?p\\_p\\_auth=iljE3giH](https://community.wolfram.com/groups/-/m/t/2576537?p_p_auth=iljE3giH)
- [7] Raymond J. Beach; A Classical Field Theory of Gravity and Electromagnetism; Journal of Modern Physics, [Vol.5 No.10, June 2014](https://doi.org/10.1098/rstl.1865.0008)
- [8] Maxwell James Clerk; A dynamical theory of the electromagnetic field; 01 January 1865; <https://royalsocietypublishing.org/doi/10.1098/rstl.1865.0008>
- [9] A. Einstein; On the Influence of Gravitation on the Propagation of Light; Annalen der Physik (ser. 4), **35**, 898–908, [http://myweb.rz.uni-augsburg.de/~eckern/adp/history/einstein-papers/1911\\_35\\_898-908.pdf](http://myweb.rz.uni-augsburg.de/~eckern/adp/history/einstein-papers/1911_35_898-908.pdf)
- [10] Mahendra Goray, Ramesh Naidu Annavarapu, [Rest mass of photon on the surface of matter](https://doi.org/10.1016/j.rinp.2019.102866), Results in Physics 16 (202) 102866, January 2020, [DOI: 10.1016/j.rinp.2019.102866](https://doi.org/10.1016/j.rinp.2019.102866)
- [11] Antonio Genova, Erwan Mazarico, Sander Goossens, Frank G. Lemoine, Gregory A. Neumann, David E. Smith & Maria T. Zuber; Solar system expansion and strong equivalence principle as seen by the NASA MESSENGER mission; Nat Commun 9; 289 (2018). [DOI: 10.1038/s41467-017-02558-1](https://doi.org/10.1038/s41467-017-02558-1)

- [12] John G. Williamson; A new linear theory of light and matter; 2019; J. Phys.: Conf. Ser. 1251 012050 DOI [10.1088/1742-6596/1251/1/012050](https://doi.org/10.1088/1742-6596/1251/1/012050)
- [13] Vegt Wim; Black Holes with Discrete Spherical Energy Levels: [https://community.wolfram.com/groups/-/m/t/2896941?p\\_p\\_auth=D7ZKuo3k](https://community.wolfram.com/groups/-/m/t/2896941?p_p_auth=D7ZKuo3k)
- [14] Vegt Wim; Time and Radius dependent GEONs with discrete Energy Levels [https://community.wolfram.com/groups/-/m/t/2900869?p\\_p\\_auth=yxR9nZu6](https://community.wolfram.com/groups/-/m/t/2900869?p_p_auth=yxR9nZu6)
- [15] Vegt Wim; Time and Angular Regions dependent GEONs with discrete energy levels. [https://community.wolfram.com/groups/-/m/t/2901457?p\\_p\\_auth=H4jjDHmQ](https://community.wolfram.com/groups/-/m/t/2901457?p_p_auth=H4jjDHmQ)
- [16] Vegt Wim; Time and Azimuthal Regions dependent GEONs with discrete energy levels [https://community.wolfram.com/groups/-/m/t/2902170?p\\_p\\_auth=yt0q5nEh](https://community.wolfram.com/groups/-/m/t/2902170?p_p_auth=yt0q5nEh)
- [17] Vegt Wim; Time, Polar Angular and Azimuthal Angular Regions dependent GEONs with discrete energy levels [https://community.wolfram.com/groups/-/m/t/2902642?p\\_p\\_auth=sW2mvv9L](https://community.wolfram.com/groups/-/m/t/2902642?p_p_auth=sW2mvv9L)
- [18] D. W. Sciama; The Physical Structure of General Relativity; Rev. Mod. Phys. 36, 463 – Published 1 January 1964; [Erratum Rev. Mod. Phys. 36, 1103 \(1964\)](#)
- [19] Adrian del Rio, Jose Navarro-Salas, and Francisco Torrenti; Renormalized stress-energy tensor for spin -1/2 fields in expanding universes; [Phys. Rev. D 90, 084017 – Published 13 October 2014](#)
- [20] Stergios Pellis; Unity Formulas for the Coupling Constants and the Dimensionless Physical Constants; Journal of High Energy Physics Gravitation and Cosmology; DOI: [10.4236/jhepgc.2023.91021](https://doi.org/10.4236/jhepgc.2023.91021)
- [21] Bloch, Yakov and Joshua Foo. “How the result of a measurement of a photon's mass can turn out to be 100.” (2023). [Corpus ID: 258426255](#)
- [22] Andrés Arámburo García, Kyrlo Bondarenko, Sylvia Ploeckinger, Josef Pradler and Anastasia Sokolenko; Effective photon mass and (dark) photon conversion in the inhomogeneous Universe; Journal of Cosmology and Astroparticle Physics, [Volume 2020, October 2020](#)
- [23] Alexander M Gabovich and Nadezhda A Gabovich; How to explain the non-zero mass of electromagnetic radiation consisting of zero-mass photons; European Journal of Physics; 2007; 28 649; DOI [10.1088/0143-0807/28/4/004](https://doi.org/10.1088/0143-0807/28/4/004)
- [24] Liang-Cheng Tu, Jun Luo and George T Gillies; The mass of the photon; Reports on Progress in Physics, Volume 68, Number 1; DOI [10.1088/0034-4885/68/1/R02](https://doi.org/10.1088/0034-4885/68/1/R02)
- [25] Doyon B; Conformal Loop Ensembles and the Stress–Energy Tensor. Lett Math Phys 103, 233–284 (2013). <https://doi.org/10.1007/s11005-012-0594-1>
- [26] T. P. Hack and V. Moretti; On the stress–energy tensor of quantum fields in curved spacetimes—comparison of different regularization schemes and symmetry of the Hadamard/Seeley–DeWitt coefficients; 2012 J. Phys. A: Math. Theor. 45 374019; DOI: [10.1088/1751-8113/45/37/374019](https://doi.org/10.1088/1751-8113/45/37/374019)
- [27] Adam Levi; Renormalized stress-energy tensor for stationary black holes;

Phys. Rev. D 95, 025007 – Published 10 January 2017;

<https://doi.org/10.1103/PhysRevD.95.025007>

[28] Gobbi, Julio; Luminiferous Ether: [General Science Journal](#); December 10, 2018  
 $\gamma_0$  = Gravitational permeability of vacuum [kg s<sup>2</sup> m<sup>-3</sup>]

[29] Xing-Hao Ye, Qiang Lin; Gravitational Lensing Analyzed by Graded Refractive Index of Vacuum; Journal of Optics A: Pure and Applied Optics; 1 May 2008; DOI [10.1088/1464-4258/10/7/075001](https://doi.org/10.1088/1464-4258/10/7/075001)

[30] Vegt Wim; “The Origin of Gravity in “Quantum Light Theory””; OSF Preprints; October 14. doi:[10.31219/osf.io/n43yd](https://doi.org/10.31219/osf.io/n43yd)

[31] P. Delva, N. Puchades, E. Schönmann, F. Dilssner, C. Courde, S. Bertone, F. Gonzalez, A. Hees, Ch. Le Poncin-Lafitte, F. Meynadier, R. Prieto-Cerdeira (et. all); Gravitational Redshift Test Using Eccentric Galileo Satellites; Phys. Rev. Lett. 121, 231101 – Published 4 December 2018; DOI: [10.1103/PhysRevLett.121.231101](https://doi.org/10.1103/PhysRevLett.121.231101)

[32] Oppenheim, Jonathan, A Postquantum Theory of Classical Gravity, Phys. Rev. X, Vol. 13, December 2023; DOI: <https://doi.org/10.1103/PhysRevX.13.041040>

[33] Vegt Wim, The Origin of Gravity, A second order Lorentz Transformation for "Accelerated Electromagnetic Fields", Generating a Gravitational Field and the property of Mass, International Research Journal of Pure and Applied Physics Vol.9 No.1, pp.12-52, 2022.

[34] Vegt Wim, The 4-Dimensional Dirac Equation in Relativistic Field Theory, European Journal of Applied Sciences, Vol 9, No. 1, pp 35 – 93, 2021

[35] Vegt Wim; A Perfect Equilibrium inside a Black Hole; Wolfram Community: [https://community.wolfram.com/groups/-/m/t/3087823?p\\_p\\_auth=dpH7iBMg](https://community.wolfram.com/groups/-/m/t/3087823?p_p_auth=dpH7iBMg)

[36] Einstein Albert; “Elementare Überlegungen zur Interpretation der Grundlagen der Quanten-Mechanik”, Translated into English, 2011, DOI: <https://doi.org/10.48550/arXiv.1107.3701>

[37] Nikko John Leo S. Lobos, Reggie C. Pantig; Generalized Extended Uncertainty Principle Black Holes: Shadow and lensing in the macro- and microscopic realms; Physics 2022, 4(4), 1318-1330; <https://doi.org/10.3390/physics4040084>

[38] Zihua Weng; Influence of velocity curl on conservation laws, October 2008, arXiv:0810.0065. <https://doi.org/10.48550/arXiv.0810.0065>

[39] Peter Vadasz; Rendering the Navier–Stokes Equations for a Compressible Fluid into the Schrödinger Equation for Quantum Mechanics, MDPI-Fluids, May 2016, <https://doi.org/10.3390/fluids1020018>

[40] Young-Sam Kwon; Asymptotic limit for rotational quantum compressible Navier–Stokes equations with multiple scales, Journal of Mathematical Analysis and Applications, Volume 464, Issue 2, 15 August 2018, Pages 1408-1424, <https://doi.org/10.1016/j.jmaa.2018.04.073>

[41] Senjo Shimizu and Hidenobu Tsuritani; On a Navier–Stokes–Ohm problem from plasma physics in multi connected domains, Partial Differential Equations and Applications (2021) 2:75, <https://doi.org/10.1007/s42985-021-00122-7>



- [42] Jean-Luc Cambier and David A. Micheletti, Theoretical Analysis of the Electron Spiral Toroid Concept , NASA/CR-2000-210654,  
<https://ntrs.nasa.gov/api/citations/20010021117/downloads/20010021117.pdf>
- [43] Sethian J.D, Obenschain S.P, Myers M, Schmitt A.J, Colombant D, Gardner J, Hegler F, Wolford M, Giuliani J, Kepple P., and Swanekamp S; Fusion energy with lasers, direct drive targets, and dry wall chambers; Nuclear Fusion, Volume 43, Number 12; [DOI 10.1088/0029-5515/43/12/015](https://doi.org/10.1088/0029-5515/43/12/015)
- [45] Jonas Degrave, Federico Felici, Jonas Buchli, Michael Neunert, Brendan Tracey, Francesco Carpanese, Timo Ewalds, Roland Hafner, Abbas Abdolmaleki, Diego de las Casas, Craig Donner, Leslie Fritz. et al; Magnetic control of tokamak plasmas through deep reinforcement learning. Nature 602, 414–419 (2022).  
<https://doi.org/10.1038/s41586-021-04301-9>
- [46] Fan, Xing-Yan, Xiang-Ru Xie, and Jing-Ling Chen. “Predicting angular-momentum waves based on Yang–Mills equations.” Results in Physics 56 (2024): 107300. DOI: <https://doi.org/10.1016/j.rinp.2023.107300>

Journal Reference